Direct georeferencing of a multi-sensor platform for mobile mapping applications and damage detection

N. Diefenbach, A. Eichhorn
Institute of Geodesy, Group of Geodetic Measuring Systems and Sensor Technology,
Technical University of Darmstadt, Franziska-Braun-Str.7, 64287 Darmstadt, Germany

Abstract. Condition monitoring of highways is an important prerequisite for timely transportation of wares. Only through early detection and rehabilitation of damaged spots of the pavement it is possible to avoid wide-ranging limitations of traffic and accompanying costly delays.

This paper presents a cost-effective realization of a vehicle-mounted multi-sensor-system for direct geo-referencing through fusion of sensor data from both an inertial measurement unit (IMU) and multiple receivers for the Global Navigation Satellite Systems (GNSS), based on an Unscented Kalman Filter (UKF).

To reduce the costs of such a system a low-cost IMU based on micro-mechanical systems (MEMS) was used. A new approach is the integration of a GNSS array consisting of four symmetrically placed antennas to determine the orientation. This leads to an increased position accuracy for the multi-sensor-system as well as an increased orientation accuracy, because all orientation angles of the platform can be introduced as additional measurements in the estimation process. Furthermore, the sensor fusion is carried out with an UKF, so that in contrast to the classic approach with an Extended Kalman Filter (EKF) the momentums of the non-linear system equations are included up to the third order.

At first the realized system is evaluated through processing in an EKF and an UKF architecture based on simulated measurements. Afterwards a real experiment confirms the advantage of orientation aided sensor fusion through a GNSS array as well as the improved logging of complex trajectories through the UKF.

Keywords. Monitoring, multi-sensor-system, Unscented Kalman Filter, road damages

1 Introduction

In the context of globalization and increasing intra-European traffic additional burdens for the German road network become obvious. As a result, adequate monitoring of the road network, consisting of a timely localisation of damages as well as documentation of the successful rehabilitation measures, is needed.

To guarantee an appropriate quality management the Federal Highway Research Institute (BASt) carries out an annual inspection of the ca. 53.000 km of Federal Highways and examines the respective road substance. To accomplish this in the given timeframe and budget appropriate measurements methods have to be chosen.

The current used technique originates from the field of Mobile Mapping. By equipping a measuring vehicle with special scanners that register the ground lengthwise and crossways to the direction of motion and can be up to 4 meters long, the kinematic detection of the street is accomplished. Additionally, the data is linked to the corresponding locality by geo-referencing through vehicle-mounted position sensors, determining the scanners position and orientation at the time of measuring (see (Paffenholz 2012)).

Due to the dimensions of the mounted sensors and the subsequent restricted maximum speed, a survey cannot be performed without interfering with the traffic flow. To solve this issue the Fraunhofer Institute of Physical Measurement Techniques (IPM) developed the Profile Pavement Scanner (PPS) (fig. 1), the first scanner to be certified by BASt for use in public spaces for this purpose.

In combination with a suitable measurement vehicle a sensor platform is created that allows for speeds of up to 100 km/h. Due to the fusion of high movement speed and the flexible deploy-
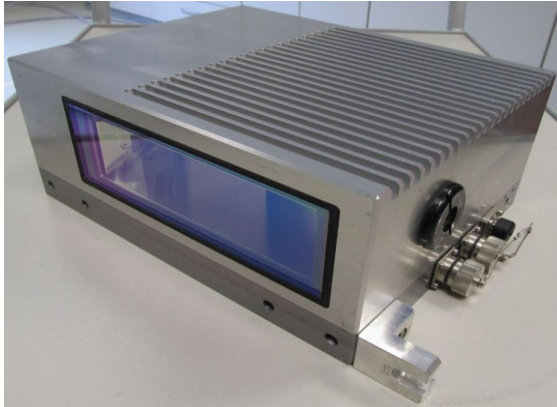
Fig. 1 Fraunhofer Profile Pavement Scanner (PPS) for pavement inspection

Fig. 2 Used GNSS-Array to determine absolute angles as observations for the sensorfusion
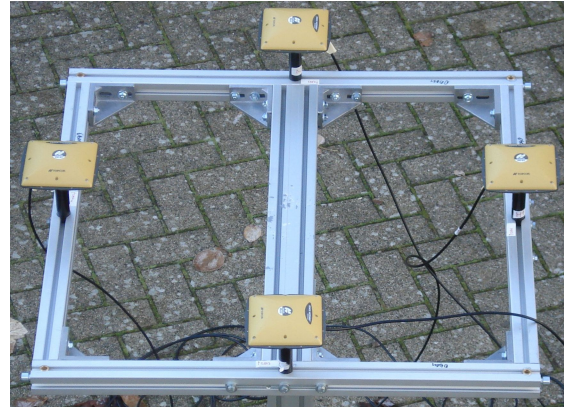
ment the documentation of the road conditions is achieved without hindering the traffic flow.

The sole positioning of the scanner could in principle be achieved by using GNSS only. But in the actual target environment signal loss due to signal shading cannot be ruled out. To deal with this and to determine the needed exterior orientation of the sensor an IMU is used as additional sensor system. Since the IMU acts as autonomous system and provides data in a high frequency independently from the GNSS receiver, it is an optimal supplement. To achieve an optimal position and orientation for the scanner, the measurements of both the IMU and GNSS sensors are combined.

This paper focuses on a fundamental case study of direct geo-referencing in post-processing as preliminary stage for the long-term objective of developing an adequate geo-referencing of highest accuracy for use with the PPS.

Consequently, different algorithms for the sensor fusion were tested with both simulated data and a practical experiment and evaluated for their suitability. Goal was to fully utilize the existing low-cost hardware and to ensure an optimal result in the sensor fusion. Therefore the state estimation is aided by a GNSS array (fig. 2), that not only allows positioning and the calculation of speed but also for the first time gives information about the orientation.

Based on the existing hardware and the intention to prevent avoidable surveys the goal was to achieve a lane precise positioning, which requires an accuracy of below 1.75 m. This is due to generate adequate approximation coordinates, which would be sufficient for the referencing of

for example an image giving sensor system.

The paper is structured as follows: After classifying this contribution in the research context of kinematic multisensory systems section 3 explains the used approaches with regards to inertial navigation and Kalman-Filters. Following this, section 4 illustrates the application and the results are compared. Finally, section 5 discusses the results.

2 Related Work

The challenge of direct geo-referencing has been approached in the early 90s (e.g. (Cannon 1991)). The focus has been the direct geo-referencing of airborne surveys (see (Skaloud 1999), (Schwarz 2001)). Therefore Cramer (2001) analysed the attainable accuracy. Basis were always high quality sensors and the EKF as fusion algorithm.

One trend in regards to algorithms was started by Julier and Uhlmann (2002) with the UKF. A comparison between UKF and EKF can be found in (Wendel et al. 2005) and (El-Sheimy, Shin, and Niu 2006). Subsequently, the emphasis changed to the realization of systems with low-cost sensors (e.g. (van der Merwe and Wan 2004) and (Shin 2005)).

Another trend in present science is the improvement of sensor fusion with more than one GNSS antenna (e.g. pioneering work by (Böder 2002), further approaches by (Wieser and Aschauer 2011), (Paffenholz 2012) and (Eling, Klingbeil, and Kuhlmann 2015)).

This paper focuses on the cost-effective realization of a multi-sensor system for direct geo-referencing based on the combination of a low-cost

MEMS-IMU and a GNSS array with four antennas. This not only allows an update of the IMU based estimations of position and velocity but also of the orientation.

Both sensors are fused in an EKF and an UKF. Based on El-Sheimy, Shin, and Niu (2006) the UKF was additionally chosen because of its ability to handle large attitude errors in an appropriate way. In this respect this paper is an extension of their contribution by concerning the assistance of the orientation estimation by using an GNSS antenna array.

In contrast to Skaloud (1999), Schwarz (2001) and Böder (2002) the sensor platform is a land-based vehicle. And unlike van der Merwe and Wan (2004) a GNSS array instead of a single antenna is used. Furthermore, the results from the UKF are compared to those of the EKF. The difference to Wendel et al. (2005) lies in the use of a loosely coupled architecture for the sensor fusion.

3 Methods

In this section the basic principles of inertial navigation, as well as EKF and UKF are explained.

3.1 Inertial Navigation

To describe the movement of a sensor platform with IMU measurements the formulation in the local, topocentric navigational coordinate system is chosen (see also (Wendel et al. 2005)). This results in navigation equations that are shown in the equations (1)-(8). To indicate the position in a higher coordinate system the WGS-84 ellipsoid in combination with latitude, longitude and elevation φ, λ and h are used. R_n and R_e describe the corresponding ellipsoidal half-axes and $v_{eb,d}^n$ the sensor platforms speed along the local vertical direction.

$$\dot{\varphi} = \frac{1}{R_n(\varphi) - h} \qquad (1)$$

$$\dot{\lambda} = \frac{1}{(R_e(\varphi) - h)\cos(\varphi)} \qquad (2)$$

$$\dot{h} = v_{eb,d}^n \qquad (3)$$

The differential equation for the speed follows as

$$\dot{\mathbf{v}}_{eb}^n = \mathbf{R}_b^n\,\mathbf{a}_{ib}^b - (2\,\boldsymbol{\omega}_{ie} + \boldsymbol{\omega}_{en}) \times \mathbf{v}_{eb}^n + \mathbf{g}_l^n \quad (4)$$

Here $\mathbf{R}_b^n$ is the rotation matrix from the body fixed in the navigational coordinate system and $\mathbf{a}_{ib}^b$ is the measured acceleration. Furthermore $\boldsymbol{\omega}_{ie}^n$ describes earth's rotation rate, $\boldsymbol{\omega}_{en}^n$ is the transportation rate and $\mathbf{g}_l^n$ is the local gravity vector.

$$\mathbf{g}_l^n = \big(0, 0, g(\varphi, h)\big)^T \qquad (5)$$

The gravity vector is not assumed as a constant and instead depends on the longitude λ and the ellipsoidal height h. The calculation follows the normal gravity formula after Somigliana (see (Torge 2002)).

The last navigation equation is the equation of orientation.

$$\dot{\boldsymbol{\Psi}}^n = \mathbf{R}_b^n\,\boldsymbol{\omega}_{ib}^b - \boldsymbol{\omega}_{ie}^n - \boldsymbol{\omega}_{en}^n \qquad (6)$$

The equations 4 and 6 need the earth rotation and the transportation rate. Those can be formulated in the navigational coordinate system as

$$\boldsymbol{\omega}_{ie}^n = \begin{bmatrix} \omega_e\cos(\varphi) & 0 & -\omega_e\sin(\varphi) \end{bmatrix}^T \quad (7)$$

and as

$$\boldsymbol{\omega}_{en}^n = \left[\frac{v_{eb,east}^n}{R_e(\varphi) - h} \quad -\frac{v_{eb,north}^n}{R_n(\varphi) - h} \quad -\frac{v_{eb,east}^n\,\tan(\varphi)}{R_e(\varphi) - h} \right]^T \tag{8}$$

3.2 Kalman-Filters

This by Rudolf Emil Kalman described algorithm is used for optimal estimations of the state in a linear or linearised system based on measurement data (see (Kalman 1960)). A distinction is made between the prediction, based on the system equation (9), and the filtering, based on the measurement equation (10).

$$\tilde{\mathbf{x}} = \mathbf{T}\tilde{\mathbf{x}} + \mathbf{B}\tilde{\mathbf{u}} + \mathbf{S}\mathbf{w} \qquad (9)$$

$$\tilde{\mathbf{l}} = \mathbf{A}\tilde{\mathbf{x}} \qquad (10)$$

The matrix $\mathbf{T}$ describes the transition matrix, $\mathbf{x}$ the state vector, $\mathbf{B}$ the outer input matrix, $\mathbf{u}$ the outer input vector, $\mathbf{S}$ the noise matrix, $\mathbf{w}$ the noise vector, $\mathbf{l}$ the measurement vector and $\mathbf{A}$ the design matrix. The system and the measurements are subject to noise that within the algorithm is referred to as Gaussian White Noise (GWN).

In the prediction step the state $\mathbf{x}$ is extrapolated based on the corresponding variance propagation $\mathbf{Q}_{\hat{\mathbf{x}}\hat{\mathbf{x}}}$. In the filtering step a control and

correction takes place by determining the covariance matrix of the innovation $\mathbf{D}$ and the Gain matrix $\mathbf{K}$. Based on these the weighted mean of the innovation between the measurement $\mathbf{l}$ and the predicted state $\bar{\mathbf{x}}$ can be computed. In another step the corresponding variance-covariance-matrix (VCM) $\mathbf{Q}_{\hat{\mathbf{x}}\hat{\mathbf{x}}}$ can be calculated.

3.2.1 Extended Kalman-Filter

Since the Kalman-Filter loses the characteristic of a Best Linear Unbiased Estimator (BLUE) when used with nonlinear problems a linearisation of the nonlinear transfer function $\mathbf{f}$ is needed (see (Eichhorn 2005) and (Paffenholz 2012)).

$$\mathbf{T}_{k+1,k} = \left.\frac{\partial \mathbf{f}_{k+1,k}(\mathbf{x}_k, \mathbf{u}_k, \mathbf{w}_k)}{\partial \mathbf{x}_k}\right|_{\mathbf{x}_k=\hat{\mathbf{x}}_k} \quad (11)$$

$$\mathbf{B}_{k+1,k} = \left.\frac{\partial \mathbf{f}_{k+1,k}(\mathbf{x}_k, \mathbf{u}_k, \mathbf{w}_k)}{\partial \mathbf{u}_k}\right|_{\mathbf{u}_k=\mathbf{u}_k} \quad (12)$$

$$\mathbf{S}_{k+1,k} = \left.\frac{\partial \mathbf{f}_{k+1,k}(\mathbf{x}_k, \mathbf{u}_k, \mathbf{w}_k)}{\partial \mathbf{w}_k}\right|_{\mathbf{w}_k=\mathbf{w}_k} \quad (13)$$

$$\mathbf{A}_{k+1,k} = \left.\frac{\partial \mathbf{h}_{k+1,k}(\mathbf{x}_{k+1}, \mathbf{v}_{k+1})}{\partial \mathbf{x}_{k+1}}\right|_{\mathbf{x}_{k+1}=\bar{\mathbf{x}}_{k+1}} \quad (14)$$

3.2.2 Unscented Kalman-Filter

An alternative approach to use a Kalman-Filter with a nonlinear problem was publicized by Julier, Uhlmann, and Durrant-Whyte (1995). The UKF is a special case of the Monte Carlo Simulation that allows updating the mean value and the VCM of a state based on deterministically chosen sigma points. The used number of sigma points is variable and can be chosen based on the application (see (Julier and Uhlmann 2002) and (Julier 2003)).

The advantage of this approach is that the nonlinear functions from the prediction as well as the measurement equations can be used directly and therefore making linearisation unnecessary. Additionally, it has to be noticed that moments up to third order are included in the UKF approach.

This paper uses the scaled unscented transformation (see (Julier 2002)), since it allows for adaption of scattering range and weightings. For the distribution of the sigma points both (Julier 2002) and (van der Merwe and Wan 2004) recommend the parameters $\alpha = 10^{-3}$, $\beta = 2$ and $\kappa = 0$ based on the assumption of normally distributed errors. The number of points should be $2n + 1$ with $n = rg(\mathbf{x})$. Initially the scaling parameter λ_{UKF} has to be calculated

$$\lambda_{\mathrm{UKF}} = \alpha^2(n + \kappa) - n \quad (15)$$

With it the sigma points of the prediction follow as

$$\boldsymbol{\mathcal{X}}_0 = \hat{\mathbf{x}} \quad (16)$$

$$\boldsymbol{\mathcal{X}}_i = \hat{\mathbf{x}} + \left(\sqrt{(n + \lambda_{\mathrm{UKF}})\,\mathbf{Q}_{\hat{\mathbf{x}}\hat{\mathbf{x}}}}\right)_i \quad (17)$$
$$i = 1, \ldots, n$$
$$\boldsymbol{\mathcal{X}}_i = \hat{\mathbf{x}} - \left(\sqrt{(n + \lambda_{\mathrm{UKF}})\,\mathbf{Q}_{\hat{\mathbf{x}}\hat{\mathbf{x}}}}\right)_i \quad (18)$$
$$i = n + 1, \ldots, 2n$$

Furthermore, the corresponding equations are distinguished by the weights of the mean value $\mathbf{W}^m$ and those of the VCM $\mathbf{W}^c$.

$$\mathbf{W}_0^m = \frac{\lambda_{\mathrm{UKF}}}{(n + \lambda_{\mathrm{UKF}})} + (1 - \alpha^2 + \beta) \quad (19)$$

$$\mathbf{W}_0^c = \frac{\lambda_{\mathrm{UKF}}}{(n + \lambda_{\mathrm{UKF}})} \quad (20)$$

$$\mathbf{W}_i^m = \mathbf{W}_i^c = \frac{\lambda_{\mathrm{UKF}}}{2(n + \lambda_{\mathrm{UKF}})} \quad (21)$$

Following this the sigma points of the prediction step are transferred with the nonlinear system equation $f()$.

$$\mathbf{y}_P = f(\boldsymbol{\mathcal{X}}_P) \quad (22)$$

Based on that the predicted state is calculated from the weighted mean .

$$\bar{\mathbf{x}} = \sum_{i=1}^{2n} \mathbf{W}_i^c\, \mathbf{y}_{\mathbf{P}_i} \quad (23)$$

The corresponding VCM results from the variance of the transferred sigma points. Due to the assumption of GWN the noise term $\mathbf{Q}$ is added.

$$\mathbf{Q}_{\bar{\mathbf{x}}\bar{\mathbf{x}}} = \left(\frac{1}{2n} \sum_{i=1}^{2n} \mathbf{W}_i^c(\mathbf{y}_{\mathbf{P}_i} - \bar{\mathbf{x}})(\mathbf{y}_{\mathbf{P}_i} - \bar{\mathbf{x}})^T\right) + \mathbf{Q}_k \quad (24)$$

For the filtering step the calculations are analogical to those of the prediction step. The sigma points are transferred based on the nonlinear measurement $h()$.

$$\mathbf{y}_F = h(\boldsymbol{\mathcal{X}}_F) \quad (25)$$

In the same way the weighted mean value and the VCM $\mathbf{Q}_{\mathrm{yy}}$ of the transferred sigma points are

calculated. The cross-correlation matrix $\mathbf{Q_{xy}}$ is determined here, too.

$$\bar{\mathbf{y}}_F = \sum_{i=1}^{2n} \mathbf{W}_i^m \; \mathbf{y_F} \qquad (26)$$

$$\mathbf{Q_{yy}} = \frac{1}{2n} \sum_{i=1}^{2n} \mathbf{W}_i^c \, (\mathbf{y_{F_i}} - \bar{\mathbf{y}}_F)(\mathbf{y_{F_i}} - \bar{\mathbf{y}}_F)^T \qquad (27)$$

$$\mathbf{Q_{xy}} = \frac{1}{2n} \sum_{i=1}^{2n} \mathbf{W}_i^c \, (\mathbf{x_{F_i}} - \bar{\mathbf{x}}_F)(\mathbf{y_{F_i}} - \bar{\mathbf{y}}_F)^T \qquad (28)$$

Parallel to the prediction the filtering takes the measurement noise $\mathbf{Q_{ll}}$ as additive term into account.

$$\mathbf{D} = \mathbf{Q_{yy}} + \mathbf{Q_{ll}} \qquad (29)$$

In contrast to the EKF the Gain matrix $\mathbf{K}$ is calculated by multiplying the covariance matrix with the inverse cofactor matrix of the innovation.

$$\mathbf{K} = \mathbf{Q_{xy}} \; \mathbf{D}^{-1} \qquad (30)$$

The final calculation of the filtered state and the filtered VCM are analogical to those of the EKF.

$$\hat{\mathbf{x}} = \bar{\mathbf{x}} + \mathbf{K} \; (\mathbf{l} - \mathbf{A} \; \bar{\mathbf{y}}_F) \qquad (31)$$

$$\mathbf{Q_{\hat{x}\hat{x}}} = \mathbf{Q_{\bar{x}\bar{x}}} - \mathbf{KDK}^T \qquad (32)$$

4 Application

To minimize the cost for the system a MEMS-IMU of the type SBG System IG-500E, with the specifications as show in table 1 and a sample rate of 20 Hz, was used.

Table 1 Specification of the IMU SBG IG-500E

	Accelerometers	Gyrocopes
dynamic range	$\pm 5\,\mathrm{g}$	$\pm 300\,°/\mathrm{s}$
inital bias	$\pm 5\,\mathrm{mg}$	$\pm 0.5\,°/\mathrm{s}$
noise density	$0.25\mathrm{mg}/\sqrt{Hz}$	$0.05°/\mathrm{s}/\sqrt{Hz}$

The results of the factory-calibration were stored inside and automatically used to correct the raw measurements. Nevertheless since IMUs based on MEMS designs show significant offsets during use even after calibration, the state vector was augmented with the biases of the accelerometer

and gyroscopes (e.g. (Wendel 2007) and (van der Merwe and Wan 2004)).

As aiding absolute sensor a GNSS array consisting of four PG-S1 antennas and two MR-1 receivers on a quadratic platform was used. This not only allows to aid the position and velocity estimation but the orientation estimation, which otherwise can not be controlled directly. The two antennas connected to the same receiver were diametrically positioned, so that there was a lengthwise and a crossways pair. Furthermore, for the processing of the position, velocity and angular output each pair was divided into a primary and a secondary antenna. The output of the receiver contains the position and velocity of the primary and the internally calculated angle between both antennas, which could directly be used as observed quantities.

Additionally, the precision of the systems was examined to obtain a reliable stochastic model for the sensor fusion. To minimize the costs the use of SAPOS-correctional data was omitted and instead only single point code solutions were used. Consequently, the position precision was determined to $s_{pos} = 2.325\,\mathrm{m}$. For the orientation measurements the output of the receivers was compared with laser tracker measurements. The orientation precision was determined to $s_\Psi = 1.2016°$. The output rate of this absolute sensor system was 10 Hz.

4.1 Prediction

To fuse the measurements of these complimentary systems an EKF as well as an UKF, both in a loosely coupled architecture, are used.

The EKF had the design of an error state filter as described in Wendel (2007) and therefore estimates the errors produced through state estimation based on pure IMU measurements.

$$\Delta \mathbf{x} = \begin{bmatrix} \Delta\mathbf{p} & \Delta\mathbf{v} & \mathbf{\Delta\Psi} & \Delta\mathbf{b}_a & \Delta\mathbf{b}_\omega \end{bmatrix} \qquad (33)$$

In contrast to that the UKF had the design of a total state filter based on the nonlinear navigation equations and estimates the wanted quantities directly.

$$\mathbf{x} = \begin{bmatrix} \mathbf{p} & \mathbf{v} & \mathbf{\Psi} & \mathbf{b}_a & \mathbf{b}_\omega \end{bmatrix} \qquad (34)$$

While the estimation of the position and velocity in the UKF do not need special consideration, there is a challenge in the selection of orientation parameters and the modelling of the IMU error characteristics with respect to the intended task.

A proper description of the platform's orientation is given with quaternions. These have the advantage that a singularity free description of orientations is guaranteed.

Following van der Merwe and Wan (2004) for the total state UKF the nonlinear propagation equation of the quaternions is used as

$$\mathbf{q}_{k+1} = \left[\mathbf{I}\cos(s) - \frac{1}{2}\,\mathbf{\Omega}(\omega)\,\Delta t\,\frac{\sin(s)}{s}\right]\mathbf{q}_k \quad (35)$$

with

$$s = \frac{1}{2}\,\sqrt{(\omega_x\,\Delta t)^2 + (\omega_y\,\Delta t)^2 + (\omega_z\,\Delta t)^2} \quad (36)$$

and

$$\mathbf{\Omega}(\omega) = \frac{1}{2}\begin{bmatrix} 0 & \omega_x & \omega_y & \omega_z \\ -\omega_x & 0 & -\omega_z & \omega_y \\ -\omega_y & \omega_z & 0 & -\omega_x \\ -\omega_z & -\omega_y & \omega_x & 0 \end{bmatrix} \quad (37)$$

Finally a model for the IMU errors has to be chosen. In this paper it is modelled as random walk. Consequently the measurements are a superposition of the true measurements $\tilde{(.)}_{ib}^{b}$, the offsets $\mathbf{b}_{(.)}$ and the GWN $\mathbf{w}_{(.)}$.

$$\boldsymbol{a}_{ib}^{b} = \tilde{\boldsymbol{a}}_{ib}^{b} + \boldsymbol{b}_a + \mathbf{w}_a \quad (38)$$
$$\boldsymbol{\omega}_{ib}^{b} = \tilde{\boldsymbol{\omega}}_{ib}^{b} + \boldsymbol{b}_\omega + \mathbf{w}_\omega \quad (39)$$

4.2 Filtering

To be precise, the lever-arm $\mathbf{l}^b$ between the GNSS and the IMU must be taken into account by correcting the measurements of position and velocity of each main antenna according to equations (40) and (41). The corresponding lever-arms between the main antennas and the case of the IMU were determined with a laser tracker to be each $0.840\,\mathrm{m}$ $\pm\,0.002\,\mathrm{m}$ before the experiment took place.

$$\mathbf{p}_{\mathrm{IMU}_i} = \mathbf{p}_{\mathrm{GNSS}_i} - \mathbf{R}_b^n\,\mathbf{l}_i^b \quad (40)$$
$$\mathbf{v}_{\mathrm{IMU}_i} = \mathbf{v}_{\mathrm{GNSS}_i} - \mathbf{R}_b^n\,(\boldsymbol{\omega}_{ib}^{b} \times \mathbf{l}_i^b) \quad (41)$$

After relating the GNSS measurements to the IMU the respective observation equations can be generated. In case of the error state EKF, where only differences between the prediction and the measurements are processed, the corresponding observation equation results from the difference of the predicted states reduced by the averaged measurements as follows.

$$\mathbf{l}_{\mathrm{EKF}} = \begin{bmatrix} \bar{\mathbf{p}}_{\mathrm{IMU}} - \frac{1}{2}(\mathbf{p}_{\mathrm{GNSS}_1} + \mathbf{p}_{\mathrm{GNSS}_2}) \\ \bar{\mathbf{v}}_{\mathrm{IMU}} - \frac{1}{2}(\mathbf{v}_{\mathrm{GNSS}_1} + \mathbf{v}_{\mathrm{GNSS}_2}) \\ \bar{\mathbf{\Psi}}_{\mathrm{IMU}} - \mathbf{\Psi} \end{bmatrix} \quad (42)$$

In case of the UKF the measurements are directly used in the observation vector $\mathbf{l}$.

$$\mathbf{l}_{\mathrm{UKF}} = \begin{bmatrix} \frac{1}{2}(\mathbf{p}_{\mathrm{GNSS}_1} + \mathbf{p}_{\mathrm{GNSS}_2}) \\ \frac{1}{2}(\mathbf{v}_{\mathrm{GNSS}_1} + \mathbf{v}_{\mathrm{GNSS}_2}) \\ \mathbf{\Psi} \end{bmatrix} \quad (43)$$

At first simulations based on artificial data of a $7.6\,\mathrm{km}$ trajectory with variations in all orientational dimensions were carried out. Therefore the error-free accelerations and gyroscopic measurements in the named respective output rates were created and superpositioned with offsets as stated in tab. 1 and GWN as follows

$$\sigma_\Psi = 1.5\,° \quad (44)$$
$$\sigma_v = 2.5\,\mathrm{m/s} \quad (45)$$
$$\sigma_p = 2.5\,\mathrm{m} \quad (46)$$

To judge the results they were transformed to a local topocentric coordinate system with the car as origin as in Eichhorn (2005) with the lengthwise component lk, the crossways component qk and the height component h (see fig. 3).
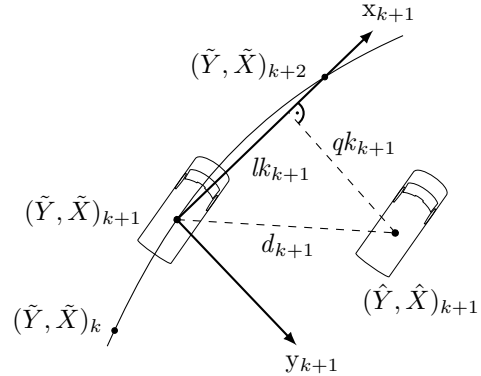
**Fig. 3** Local coordinate system as proposed by Eichhorn (2005)

The simulation showed, that the approach using the EKF resulted in a mean position deviation of $d_p = 0.796\,\mathrm{m} \pm 0.876\,\mathrm{m}$, while the approach with the UKF yielded a mean position deviation $d_p = 0.699\,\mathrm{m} \pm 0.536\,\mathrm{m}$ in post-processing. Accordingly, a significant advantage of one algorithm over the other could not be detected. After

the successful simulations a practical experiment was carried out.

The focus of this experiment was to test the system in a "high-kinematic" scenario to ensure that both the sensors and the algorithms work under extreme circumstances. Regarding the simulations the difference were the tighter turns with a partial curb turning raidus of only 10 m. The gathered data was again analysed in a post-processing step.

The reference trajectory was generated from data gathered by another multi-sensory system consisting of a navigational class iMAR iNav RQH-1003 IMU in combination with a dual band GNSS receiver with carrier-phase based correctional data. It was processed with the commercial software solution KingsPad and can be seen in fig. 4. As measurement equipment of superior category this solution has an deviation of ca. 0.002 m.
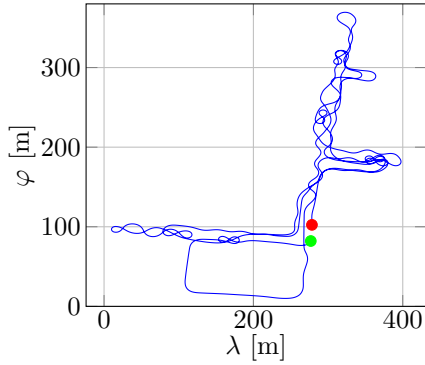
Fig. 4 Reference trajectory created with a navigational grade IMU, differential GNSS and processed with KingsPad

Due to the highly kinematic trajectory with very tight turns the EKF diverges soon after the start of the movement depending on the attitude error at initialization. But because of the high update rate of the GNSS even initialization errors of over 30° can still be compensated, but degrade the navigation solution significantly. Therefore a "pre-zero"-epoch with adjacent averaging of the measurements is required.

In contrast to that the UKF processes the data successfully and is able to compensate even large initialization errors in a minimum of time.

For an appropriate comparison and analysis of the proposed approach for each algorithm two different cases were processed: On the one hand without aiding through absolute orientation measurements and on the other hand with aiding. As appropriate operating figures the mean position

deviation with corresponding root mean square (exemplary in equations 47 and 48) were chosen.

$$\bar{\Delta}_{\text{lk}} = \frac{1}{n} \sum_{i=1}^{n} \tilde{\text{lk}}_i - \hat{\text{lk}}_i \qquad (47)$$

$$\text{rms}_{\text{lk}} = \sqrt{\frac{1}{n} \sum_{i=1}^{n} v_{\text{lk}_i}^2} \qquad (48)$$

The tables 2 and 3 summarize the results. Hereby it has to be mentioned, that the yaw angle is intentionally not listed in the tables. This is due to a problem with the mechanisation of the z-gyroscope, which led to an fluctuation range of the rms between 80°-100° in case of the unaided respectively between 10°-14° in case of the aided orientation, without significant differences between the chosen algorithms. It has to be underlined that in this case the reductions of the rms is achieved through the use of additional observation information and not through the choice of the processing algorithm. Apart from that the dimensions of the results correspond with those from the simulations.

Table 2 Results of processing the field data using the EKF

		unaided ori.		aided ori.	
		$\bar{\Delta}$	rms	$\bar{\Delta}$	rms
lk	[m]	0.620	0.449	0.575	0.386
qk	[m]	4.420	2.083	3.942	1.778
h	[m]	0.012	1.131	0.006	1.060
α	[°]	0.1457	3.5769	0.2145	1.6424
β	[°]	-2.8932	2.5899	-2.6715	1.1711

Table 3 Results of processing the field data using the UKF

|		unaided ori.		aided ori.	
		$\bar{\Delta}$	rms	$\bar{\Delta}$	rms
lk	[m]	0.724	0.449	0.675	0.500
qk	[m]	0.782	0.565	0.563	0.477
h	[m]	0.053	0.289	0.045	0.289
α	[°]	-5.6236	2.3392	0.2131	0.1503
β	[°]	-3.4452	1.1608	0.1057	0.1178

In case of the unaided orientation it can be seen, that using the EKF results in inhomogeneous estimated position components, which is

7

shown by a considerable deviation in the crossways component *qk*. In contrast to that the UKF provides a more homogeneous output regarding the lengthways and crossways components.

In case of the additional aided orientation the accuracy of the position estimations slightly improve for both algorithms. But more important the orientation estimations can be significantly improved. For the EKF the effect mainly manifests in a reduced standard deviation, while an unexpected high estimation error of the crossways component *qk* still remains. This is caused through an error in the initial point, which degrades the whole navigation solutions. In case of the UKF the additional aiding of the orientation manifests as an improvement of both the accuracy and the precision.

One reason for this outcome is found in the choice of the platform. By using a land vehicle the changes in roll and pitch are quite small compared to those in the yaw axis. Since the experiment was conducted on a trajectory with many sharp turns to ensure working algorithms, drastic changes were detected by the yaw axis gyroscope. In combination with the mechanical inconsistency the detected errors occured.

As it can be seen in table 3, the use of the UKF provides better results in post-processing. But an inspection of the associated histograms (figures 5 and 6) reveals that a normal distribution can only be assumed for modelling the orientation errors.

(a) Histogram of Δlk

(b) Histogram of Δqk

(c) Histogram of Δh
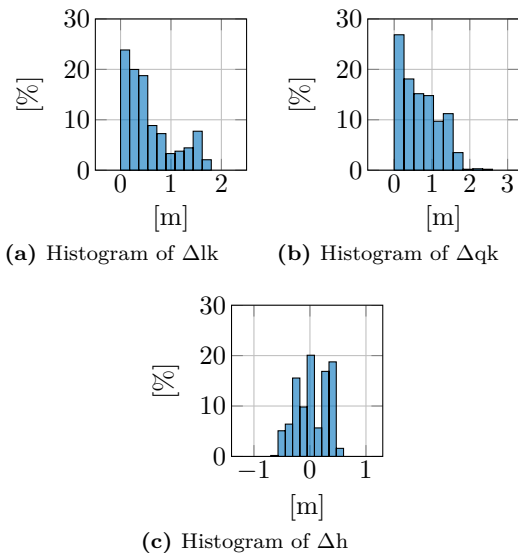
Fig. 5 Histograms of the position errors for the aided UKF result

(a) Histogram of $\Delta\alpha$
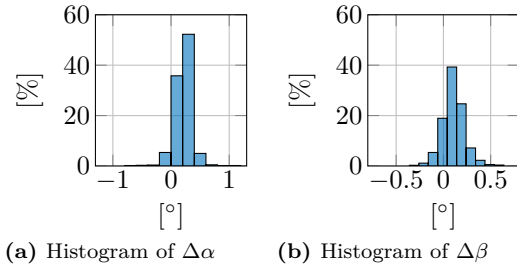
(b) Histogram of $\Delta\beta$

Fig. 6 Histograms of the orientation errors for the aided UKF result

5 Conclusion

To detect the locations in need of rehabilitation in a time- and cost-efficient way with a position in the world coordinate system a direct geo-referencing of the PPS is needed. As preliminary stage a low-cost system was successfully developed, that enables direct referencing at any given time through fusion of a GNSS array and MEMS-IMU measurements. It could be shown, that with the inclusion of the IMU as support for the GNSS array the target of a lane precise positioning could be achieved in more than 99 % of the time.

For the future development of this system, the assumption of normally distributed measurement noise has to be replaced by correlated noise and should be taken into account accordingly. Additionally, for the long-term objective of developing an adequate geo-referencing of highest accuracy for use with the PPS, changing the fusion architecture to a tight coupling, meaning a centralized processing of the raw GNSS data in the form of pseudoranging and doppler measurements, could be a promising way of maxing out the potential of the system. Furthermore, for higher accuracies, the MEMS-IMU has to be replaced with a superior sensor and differential GNSS positioning or real time GNSS corrections need to be applied.

References

Böder, Volker (2002). "Zur hochpräzisen GPS-Positions- und Lagebestimmung unter besonderer Berücksichtigung mariner Anwendungen". PhD thesis. Universität Hannover.

Cannon, M.E. (1991). *Airborne GPS/INS with Application to Aerotriangulation*. Tech. rep. (UCSE Report Nr. 20040). The University of Calgary.

Cramer, M. (2001). "Genauigkeitsuntersuchung zur GPS/INS-Integration in der Aerophotogrammetrie". PhD thesis. Universität Stuttgart.

Eichhorn, A. (2005). "Ein Beitrag zur Identifikation von dynamischen Strukturmodellen mit Methoden der adaptiven KALMAN-Filterung". PhD thesis. Universität Stuttgart.

Eling, C., L. Klingbeil, and H. Kuhlmann (2015). "A Direct Georeferencing System for Real-Time Position and Attitude Determination of Lightweight UAVS". In: *FIG Working Week 2015.*

Julier, S.J. (2002). "The scaled unscented transformation". In: *American Control Conference, 2002. Proceedings of the 2002.* Vol. 6, 4555–4559 vol.6.

– (2003). "The spherical simplex unscented transformation". In: *American Control Conference, 2003. Proceedings of the 2003.* Vol. 3, 2430–2434 vol.3.

Julier, S.J. and J.K. Uhlmann (2002). "Reduced sigma point filters for the propagation of means and covariances through nonlinear transformations". In: *American Control Conference, 2002. Proceedings of the 2002.* Vol. 2, 887–892 vol.2.

Julier, S.J., J.K. Uhlmann, and H.F. Durrant-Whyte (1995). "A new approach for filtering nonlinear systems". In: *American Control Conference, Proceedings of the 1995.* Vol. 3, 1628–1632 vol.3.

Kalman, R.E. (1960). "A New Approach to Linear Filtering and Prediction Problems". In:

Paffenholz, J.-A. (2012). "Direct Georeferencing of 3D point clouds with 3D positioning sensors". PhD thesis. Gottfried Wilhelm Leibniz Universität Hannover.

Schwarz, K.-P. (2001). *INS/GPS Integration for Geodetic Applications.* Tech. rep. University of Calgary.

El-Sheimy, N., E.-H. Shin, and X. Niu (2006). "Kalman filter face-off: Extended vs. unscented kalman filters for integrated gps and mems inertial". In: *Inside GNSS* 1.2, pp. 48–54.

Shin, E.-H. (2005). "Estimation techniques for low-cost inertial navigation". PhD thesis. University of Calgary.

Skaloud, J. (1999). "Optimizing georeferencing of airborne survey systems by INS/DGPS". PhD thesis. University of Calgary.

Torge, W. (2002). *Geodäsie.* De Gruyter.

van der Merwe, R. and E. Wan (2004). "Sigma-Point Kalman Filters for Integrated Navigation". In: *Proceedings of the 60th Annual Meeting of The Institute of Navigation (ION).*

Wendel, J. (2007). *Integrierte Navigationssysteme: Sensordatenfusion, GPS und inertiale Navigation.* Oldenbourg.

Wendel, J. et al. (2005). "Comparison of Extended and Sigma-Point Kalman Filters for Tightly Coupled GPS/INS Integration". In: *AIAA Guidance, Navigation, and Control Conference and Exhibit.*

Wieser, A. and R. Aschauer (2011). "Estimating platform kinematics using multi-antenna GNSS". In: *Österreichische Zeitschrift für Vermessung und Geoinformation (VGI), begutachteter Beitrag 99 (2011).*